HOKKAIDO UNIVERSITY

| | |
|---|---|
| Title | Role of wire core in extinction of opposed flame spread over thin electric wires |
| Author(s) | Konno, Yusuke; Hashimoto, Nozomu; Fujita, Osamu |
| Citation | Combustion and flame, 220, 7-15<br>https://doi.org/10.1016/j.combustflame.2020.06.026 |
| Issue Date | 2020-10 |
| Doc URL | https://hdl.handle.net/2115/86192 |
| Rights | © <2020>. This manuscript version is made available under the CC-BY-NC-ND 4.0 license<br>http://creativecommons.org/licenses/by-nc-nd/4.0/ |
| Rights(URL) | https://creativecommons.org/licenses/by-nc-nd/4.0/ |
| Type | journal article |
| File Information | CNF_Manuscript_final.pdf |

Hokkaido University Collection of Scholarly and Academic Papers : HUSCAP

# Role of wire core in extinction of opposed flame spread over thin electric wires

**Yusuke Konno[a], Nozomu Hashimoto[a], and Osamu Fujita[a*]**

[a]Division of Mechanical and Space Engineering, Hokkaido University,

Kita 13, Nishi 8, Kita-ku, Sapporo, Hokkaido 060-8628, Japan

[*]Corresponding Author

E-mail address: ofujita@eng.hokudai.ac.jp

Tel: +81-11-706-6385

## Abstract

Theoretical and experimental works have been carried out to clarify the effect of core material on the extinction characteristics of the flame spreading over electric wires. Additionally, an attempt has been made to explain previous experimental results (Takahashi *et al.*, 2013 [1]) which found that Limiting Oxygen Concentration (LOC) of copper (Cu) wire is higher than that of nickel-chrome (NiCr) wire. A theoretical model is developed to discuss the heat loss mechanism in the unburned zone ahead of the gas-phase preheat zone and its validity is confirmed by measured temperature profiles along Cu, iron (Fe), and NiCr wires insulated by low-density polyethylene (LDPE). The theoretical analysis reveals that the flame spread rate is a crucial value to assess the extinction characteristics of the flame spreading over electric wires because it controls heat loss in the unburned zone. The reduction of the flame spread rate increases heat loss in the unburned zone and induces the quenching extinction as a result of extended thermal diffusion length along the electric wire. It is also found that a highly conductive wire increases heat loss rather than poorly conductive wire even under the same flame spread rate. Such characteristics are well described by a newly introduced parameter, $\eta_{\mathrm{f}}$, which is a dimensionless flame spread rate derived by the present study. By using $\eta_{\mathrm{f}}$, previous experimental findings [1] are successfully explained.

**Keywords:** Electric wire; Flame spread; Extinction limit; Temperature measurement; Microgravity

## Nomenclature

| | |
|---|---|
| $A$ | cross-sectional area |
| $Bi$ | Biot number |
| $C_1,\ C_2$ | regression coefficients |
| $c$ | specific heat |
| $h_\mathrm{t}$ | heat transfer coefficient |
| $L_\mathrm{c}$ | effective heat-diffusion length along the wire core |
| $Nu$ | Nusselt number |
| $P$ | perimeter |
| $Pe$ | Péclet number |
| $\dot{Q}_\mathrm{enth}$ | enthalpy change of the wire core and insulation |
| $\dot{Q}_\mathrm{cond}$ | forward heat conduction through the wire core |
| $\dot{Q}_\mathrm{loss}$ | heat loss at the surface of the insulation |
| $\dot{q}''_\mathrm{cs}$ | heat flux at the interface between the wire core and insulation |
| $Re$ | Reynolds number |
| $r$ | radius |
| $T$ | temperature |
| $V_\mathrm{f}$ | flame spread rate |
| $V_\mathrm{f,crit}$ | critical flame spread rate |
| $V_\mathrm{g}$ | airflow velocity |

| | |
|---|---|
| $x$ | x coordinates |

*Greek*

| | |
|---|---|
| $\alpha$ | thermal diffusivity |
| $\varepsilon$ | emissivity |
| $\eta_{\mathrm{f}}$ | dimensionless flame spread rate |
| $\lambda$ | thermal conductivity |
| $\nu$ | kinematic viscosity |
| $\rho$ | density |
| $\sigma$ | Stefan-Boltzmann coefficient |
| $\phi$ | dimensionless heat transfer term |

*Subscript*

| | |
|---|---|
| c | wire core |
| g | gas |
| s | insulation |
| w | electric wire (wire core and insulation) |
| $\infty$ | ambient condition |

## 1. Introduction

The combustion of electric wires is the most probable cause of fire in human space activities [2]. Therefore, research on the flammability of electric wires under various conditions attained in spacecraft is essential as a basis of spacecraft fire safety. For this reason, many studies on wire combustion in microgravity have been carried out regarding flame spread [3][4][5][6][7][8][9], and its extinction phenomena [1][10][11][12], while the ground-based test standard for the flammability of electric wires is available [13].

Electric wires consist of a metal conductor and flammable polymer coating which is a unique feature of electric wires. There have been numerous researches investigating the role of the metal conductor on the flammability of electric wires and an excellent review is also available [14]. Bakhman *et al.* [15] studied flame spread over a polymeric coating on copper (Cu) wires and glass threads and revealed that a highly conductive wire can increase the flame spread rate ($V_\mathrm{f}$). Nakamura *et al.* [16][17] studied the effect of ambient pressure on flame spread over low-density polyethylene (LDPE) insulated iron (Fe) and nickel-chrome (NiCr) wires in horizontal configuration under normal gravity. They also showed that a highly conductive wire can lead to greater $V_\mathrm{f}$, and that $V_\mathrm{f}$ for NiCr wire increases with decreasing ambient pressure, whereas $V_\mathrm{f}$ for Fe wire remains almost constant as a function of pressure. These trends are explained by the pressure dependence of the effective heat-diffusion length $L_\mathrm{g}$ in the gas phase and $L_\mathrm{c}$ along the wire core. When $L_\mathrm{g} > L_\mathrm{c}$ $\left(L_\mathrm{g} < L_\mathrm{c}\right)$ a flame-driven mode (wire-driven mode) is attained.

Takahashi *et al.* [1] obtained the Limiting Oxygen Concentrations (LOCs) of opposed-flow flame spread over LDPE-insulated Cu and NiCr wires in both microgravity and normal gravity with horizontal configuration. They found that both tested wires showed smaller LOC in microgravity than in normal gravity. These trends are qualitatively consistent with previous studies on the flame spread limits of thin cellulosic paper [18] and PMMA sheet [19][20]. More interestingly, they reported that the flame spreading over NiCr wire is sustained at lower oxygen concentration than that over Cu wire in both microgravity and normal gravity. Their result implies that highly conductive wire suppresses the flammability of insulation materials at near-extinction conditions; nevertheless, many studies report that highly conductive wire increases $V_{\mathrm{f}}$. Hu *et al*. [21] systematically investigated the effect of sample orientation on the flame spread over the same wire sample used by Takahashi *et al.* [1]. They found that $V_{\mathrm{f}}$ for Cu wire becomes much faster than that for NiCr wire in downward configuration. However, as the orientation of the wire sample approaches the horizontal, $V_{\mathrm{f}}$ for Cu wire monotonically decreases, whereas $V_{\mathrm{f}}$ for NiCr wire remains nearly constant. As a result, the difference between $V_{\mathrm{f}}$ for Cu and NiCr becomes small in horizontal configuration. Konno *et al.* [22] investigated how the ambient oxygen concentration affects flame spread over LDPE-insulated Cu and NiCr wires in downward configuration under normal gravity. They also confirmed that a highly conductive wire increases $V_{\mathrm{f}}$ and demonstrated that flame length plays a significant role in the flame-spreading process because of the presence of a metal conductor behind the burnout edge of the insulation material. Additionally, they found that flame spreading over Cu wire is sustained at lower

oxygen concentration than that over NiCr wire. Interestingly, this trend is inconsistent with the result obtained by Takahashi *et al.* [1] and suggests that heat conduction in a wire core during flame spread process has different effects on the extinction limits depending on the surrounding flow field.

Despite there are many studies on the flammability of electric wires as introduced above, research on the effect of the core material on the flame spreading over electric wires under near-extinction conditions is very limited. In fact, no clear explanation regarding why the LOC of Cu wire exceeds that of NiCr wire in horizontal spread under both microgravity and normal gravity is available, whereas the opposite was observed in downward spread under normal gravity. To address the question, the present study proposes a theoretical description of how heat conduction through a wire core affects flame spread and its extinction in electric wires. In particular, we focus on the flame-extinction mechanism under the condition of *large Damköhler number*, where heat loss generally dominates flame extinction [23][24][25][26]. The analysis thus intentionally ignores how finite-rate chemical kinetics affects flame spreading over an electric wire. Considering the importance of the heat loss mechanism in the unburned part of an electric wire, we predict the temperature profile along an electric wire with the theoretical model. Then, the variation of heat loss depending on the core material is evaluated under the supports of experimental observation.

## 2. Heat-transfer analysis

### *2.1. Coupled energy-balance equation of electric wire*

We begin with a theoretical description of the heat-transfer mechanism in the unburned zone during flame spread over an electric wire. Figure 1 shows a conceptual description of opposed-flame spread over an electric wire and the temperature profile along a wire core during flame spread. The unburned zone in the figure indicates that the upstream side beyond the preheat zone characterized by gas-phase heat conduction. Therefore, the electric wire in the unburned zone is assumed to be exposed to ambient temperature external airflow.

For simplicity, we make the following assumptions: (i) the flame spreads in steady-state, (ii) the flame shape is axisymmetric around the wire, (iii) the flame location is fixed in the coordinate system (iv) the electric wire is sufficiently long that end effects are negligible, (v) both the wire core and insulation are sufficiently thin to be treated as thermally thin solids, (vi) the axial heat conduction in the insulation is ignored because the insulation is thin and its thermal conductivity is much smaller than that of the wire core, (vii) both the wire core and insulation are in perfect thermal contact, and (viii) the physical properties of the wire core and insulation are assumed to be independent of temperature. With these assumptions, the energy-balance equations for a wire core and insulation are

$$\rho_{\mathrm{c}} c_{\mathrm{c}} A_{\mathrm{c}} (-V_{\mathrm{f}}) \frac{\mathrm{d}T_{\mathrm{c}}}{\mathrm{d}x} = A_{\mathrm{c}} \lambda_{\mathrm{c}} \frac{\mathrm{d}^2 T_{\mathrm{c}}}{\mathrm{d}x^2} - P_{\mathrm{c}} \dot{q}''_{\mathrm{cs}}, \tag{1}$$

$$\rho_{\mathrm{s}} c_{\mathrm{s}} A_{\mathrm{s}} (-V_{\mathrm{f}}) \frac{\mathrm{d}T_{\mathrm{s}}}{\mathrm{d}x} = P_{\mathrm{c}} \dot{q}''_{\mathrm{cs}} - P_{\mathrm{s}} h_{\mathrm{t}} (T_{\mathrm{s}} - T_{\infty}), \tag{2}$$

where the subscripts c, s, g, and $\infty$ denote the wire core, the insulation, the gas phase, and the ambient condition, respectively. In Eqs. (1) and (2), $\rho$ is the density, $c$ is the specific heat, $A$ is the cross-sectional area, $V_{\mathrm{f}}$ is the flame-spread rate, $T$ is the temperature, $\lambda$ is the thermal conductivity, $P$ is the perimeter, $\dot{q}''_{\mathrm{cs}}$ is the heat flux at the interface between the wire core and insulation, and $h_{\mathrm{t}}$ is the heat-transfer coefficient to the surroundings. To include the radiation effect at the surface of the insulation, $h_{\mathrm{t}}$ takes the form

$$h_{\mathrm{t}} = \frac{Nu\lambda_{\mathrm{g}}}{2r_{\mathrm{s}}} + 4\varepsilon_{\mathrm{s}}\sigma T_{\infty}^{3}, \tag{3}$$

where $Nu = 0.32 + 0.155Re^{0.50}$ [27] and $Re = 2r_{\mathrm{s}}V_{\mathrm{g}}/\nu_{\mathrm{g}}$. Here, $Nu$ is the Nusselt number, $r$ is the radius, $\varepsilon$ is the emissivity, $\sigma$ is the Stefan-Boltzmann coefficient, $Re$ is the Reynolds number, $V_{\mathrm{g}}$ is the airflow velocity, and $\nu$ is the kinematic viscosity. Note that $Nu$ in Eq. (3) can be used for a thin cylinder in a co-axial flow field [27].

A complete description of the heat-transfer process in an electric wire requires a multi-temperature model that simultaneously tracks $T_{\mathrm{c}}$ and $T_{\mathrm{s}}$ in Eqs. (1) and (2). However, to simplify the problem we assume that the axial temperature profile in the unburned insulation is the same as in the wire core, which allows a single temperature model to be adopted. Combining Eqs. (1) and (2) with the assumption that $T_{\mathrm{c}} = T_{\mathrm{s}} = T_{\mathrm{w}}$, we obtain the following coupled energy-balance equation:

$$(\rho_c c_c A_c + \rho_s c_s A_s)(-V_f)\frac{dT_w}{dx} = A_c \lambda_c \frac{d^2 T_w}{dx^2} - P_s h_t (T_w - T_\infty). \tag{4}$$

Equation (4) is a homogeneous, linear, second-order differential equation with constant coefficients, so an analytical solution describing the temperature profile along an electric wire can be obtained by applying the appropriate boundary conditions.

*2.2. Temperature profile and effective heat-diffusion length along wire core*

To solve Eq. (4), we apply the following boundary conditions:

$$x = 0,\ T_w = T_u \ \text{ and } \ x = \infty,\ T_w = T_\infty. \tag{5}$$

$x = 0$ corresponds to the front of the preheat zone as described in Fig. 1. $T_u$ in Eq. (5) depends on the heat transfer in the downstream side of the unburned zone and it is left as an unknown quantity in the analysis. With these boundary conditions, the temperature profile along the electric wire in the unburned zone is

$$T_w = T_\infty + (T_u - T_\infty)\exp\left(-\frac{x}{L_c}\right), \tag{6}$$

where

$$L_{\mathrm{c}} \equiv 2\left[\frac{V_{\mathrm{f}}}{\alpha_{\mathrm{w}}} + \left(\left(\frac{V_{\mathrm{f}}}{\alpha_{\mathrm{w}}}\right)^2 + \frac{4P_{\mathrm{s}}h_{\mathrm{t}}}{A_{\mathrm{c}}\lambda_{\mathrm{c}}}\right)^{1/2}\right]^{-1}, \tag{7}$$

$$\alpha_{\mathrm{w}} \equiv \frac{A_{\mathrm{c}}\lambda_{\mathrm{c}}}{\rho_{\mathrm{c}}c_{\mathrm{c}}A_{\mathrm{c}} + \rho_{\mathrm{s}}c_{\mathrm{s}}A_{\mathrm{s}}}. \tag{8}$$

$L_{\mathrm{c}}$ in Eq. (7) is defined as "effective heat-diffusion length along a wire core" which is an important characteristic length to discuss the heat transfer mechanism in the unburned zone. As shown by Eq. (7), $L_{\mathrm{c}}$ increases with decreasing $V_{\mathrm{f}}$ or with increasing $\lambda_{\mathrm{c}}$. In other words, the temperature profile in the unburned zone extends in the upstream direction as $V_{\mathrm{f}}$ decreases and this effect becomes more pronounced as $\lambda_{\mathrm{c}}$ increases. Note also that the elongation of the temperature profile in the unburned zone contributes to the flame-spread process via two factors: (i) it raises the enthalpy of the unburned insulation before the unburned wire goes into the preheat zone, and (ii) it increases the heat loss from the surface of the unburned insulation to the ambient. Therefore, it is interesting to know how effectively the heat transported to the unburned zone is recirculated into the unburned insulation to promote the flame-spread process.

*2.3. Controlling mechanism of heat loss in the unburned zone*

The macroscopic energy-balance equation in the unburned zone is derived by integrating Eq. (4) from $0$ to $\infty$. The result is

$$\dot{Q}_{\mathrm{cond}} = \dot{Q}_{\mathrm{enth}} + \dot{Q}_{\mathrm{loss}}, \tag{9}$$

where

$$\dot{Q}_{\mathrm{cond}} = \int_0^{\infty} A_{\mathrm{c}}\lambda_{\mathrm{c}} \frac{\mathrm{d}^2 T_{\mathrm{w}}}{\mathrm{d}x^2}\,\mathrm{d}x = \frac{A_{\mathrm{c}}\lambda_{\mathrm{c}}(T_{\mathrm{u}} - T_{\infty})}{L_{\mathrm{c}}}, \tag{10}$$

$$\dot{Q}_{\mathrm{enth}} = \int_0^{\infty} (\rho_{\mathrm{c}} c_{\mathrm{c}} A_{\mathrm{c}} + \rho_{\mathrm{s}} c_{\mathrm{s}} A_{\mathrm{s}})(-V_{\mathrm{f}}) \frac{\mathrm{d}T_{\mathrm{w}}}{\mathrm{d}x}\,\mathrm{d}x = (\rho_{\mathrm{c}} c_{\mathrm{c}} A_{\mathrm{c}} + \rho_{\mathrm{s}} c_{\mathrm{s}} A_{\mathrm{s}}) V_{\mathrm{f}} (T_{\mathrm{u}} - T_{\infty}), \tag{11}$$

$$\dot{Q}_{\mathrm{loss}} = \int_0^{\infty} P_{\mathrm{s}} h_{\mathrm{t}} (T_{\mathrm{w}} - T_{\infty})\,\mathrm{d}x = P_{\mathrm{s}} h_{\mathrm{t}} L_{\mathrm{c}} (T_{\mathrm{u}} - T_{\infty}). \tag{12}$$

$\dot{Q}_{\mathrm{cond}}$ is the forward heat conduction through the wire core, $\dot{Q}_{\mathrm{enth}}$ is the enthalpy change of the electric wire in the unburned zone, and $\dot{Q}_{\mathrm{loss}}$ is the heat loss at the surface of the unburned insulation. To evaluate the relative importance of $\dot{Q}_{\mathrm{loss}}$ and $\dot{Q}_{\mathrm{enth}}$, they are normalized as $\phi_{\mathrm{loss}} \equiv \dot{Q}_{\mathrm{loss}}/\dot{Q}_{\mathrm{cond}}$ and $\phi_{\mathrm{enth}} \equiv \dot{Q}_{\mathrm{enth}}/\dot{Q}_{\mathrm{cond}}$. Substituting Eqs. (10), (11), and (12) into $\phi_{\mathrm{loss}}$ and $\phi_{\mathrm{enth}}$, we obtain

$$\phi_{\mathrm{loss}} = \frac{P_{\mathrm{s}} h_{\mathrm{t}} L_{\mathrm{c}}^2}{A_{\mathrm{c}}\lambda_{\mathrm{c}}} \quad \text{and} \quad \phi_{\mathrm{enth}} = \frac{V_{\mathrm{f}} L_{\mathrm{c}}}{\alpha_{\mathrm{w}}}. \tag{13}$$

As can be seen in Eq. (13), $T_{\mathrm{u}}$ is eliminated thanks to the normalization. Thus, we can now consider the heat transfer mechanism in the unburned zone without giving $T_{\mathrm{u}}$. Note also that $\phi_{\mathrm{loss}}$ and $\phi_{\mathrm{enth}}$ correspond to the Biot number ($Bi$) and Péclet number ($Pe$) in the system, respectively. Here, we

define the $V_\mathrm{f}$ at $\phi_\mathrm{loss} = \phi_\mathrm{enth}$ (or $\dot{Q}_\mathrm{loss} = \dot{Q}_\mathrm{enth}$) as the critical flame spread rate $V_\mathrm{f,crit}$. Substituting Eq. (13) into $\phi_\mathrm{loss} = \phi_\mathrm{enth}$, we obtain $V_\mathrm{f,crit}$ as follow

$$V_\mathrm{f,crit} = \left[\frac{A_\mathrm{c}\lambda_\mathrm{c}P_\mathrm{s}h_\mathrm{t}}{2(\rho_\mathrm{c}c_\mathrm{c}A_\mathrm{c} + \rho_\mathrm{s}c_\mathrm{s}A_\mathrm{s})^2}\right]^{1/2}. \tag{14}$$

Figure 2 plots $\phi_\mathrm{loss}$ and $\phi_\mathrm{enth}$ against the normalized flame-spread rate $\eta_\mathrm{f} \equiv V_\mathrm{f}/V_\mathrm{f,crit}$. The results show that a decrease in $\eta_\mathrm{f}$ increases $\phi_\mathrm{loss}$ and reduces $\phi_\mathrm{enth}$. From the figure, it is found that $V_\mathrm{f}$ itself is an essential value that controls heat loss in the unburned zone and we can understand that reducing $V_\mathrm{f}$ makes it harder to sustain the flame spread because of the increased $\phi_\mathrm{loss}$. For example, as Fig. 2 naturally tells that when $V_\mathrm{f}$ falls below $V_\mathrm{f,crit}$ ($\eta_\mathrm{f} < 1$), more than 50% of the heat transported to the unburned zone is lost to the ambient to cool the electric wire. In other words, a decrease in $V_\mathrm{f}$ induces the quenching extinction of the flame spreading over electric wires. Furthermore, the analysis presented here suggests that there is a minimum $V_\mathrm{f}$ which can maintain the steady-state before the extinction limit is found.

Some more important insights are given from the relationship between $\eta_\mathrm{f}$ and $\phi_\mathrm{loss}$. As shown by Eq. (14), an increase in $\lambda_\mathrm{c}$ increases $V_\mathrm{f,crit}$, which suggests that, even if $V_\mathrm{f}$ of a higher conductive wire is greater than that of a lower conductive wire, the former can result in larger $\phi_\mathrm{loss}$ because $V_\mathrm{f,crit}$ increases with an increase in $\lambda_\mathrm{c}$ then reduce $\eta_\mathrm{f}$. Namely, it can be considered that $\eta_\mathrm{f}$ is a real parameter that evaluates the heat loss in the unburned zone and the quenching extinction.

## 3. Experiment

To verify the model proposed in section 2, temperature data were acquired by fixing a fine TC on the surface of a wire core. The time-dependent temperature change was determined when the spreading flame crossed the position of the TC. The experiments were conducted in downward configuration to keep the flame spread phenomenon as an axisymmetric state. Figure 3(a) shows the experimental apparatus used in this study, which is similar to the apparatus used in a previous study [22]. The test section consists of a 500-mm-long acrylic tube with an inner diameter of 60 mm. Mass-flow controllers controlled the flow rate of the oxygen and nitrogen gas mixture in the test section. The gas mixture was supplied uniformly to the test section through a bed of glass beads and a honeycomb at the bottom of the flow duct, and the wire sample was supported vertically at the center of the test section. The upper section of the wire sample was ignited by an electrically heated Kanthal wire coil, and the spreading flame was recorded by a digital video camera. A 0.1-mm-diameter K-type TC was fixed to the surface of the wire core, as shown in Figs. 3(b) and 3(c), and the temperature history of the wire core was recorded by using a data logger with a sampling rate of 100 Hz.

The wire samples used in this study were manufactured for laboratory experiments. LDPE was chosen as insulation material, and three types of wire cores—Cu, Fe, and NiCr—were used to investigate the effects of the thermal conductivity of the wire core. Table 1 lists the physical properties of the sample materials. The diameter of each wire core is 0.50 mm and the LDPE insulation is 0.15-mm thick. Experiments were conducted with oxygen concentrations in the range of 16–25 vol% and

**Table 1** Properties of LDPE, Cu, Fe, and NiCr.

| | LDPE | Cu | Fe | NiCr |
|---|---|---|---|---|
| Density, kg/m$^3$ | 920 | 8890 | 7850 | 7850 |
| Specific heat, J/(kg·K) | 2300 | 385.1 | 475.1 | 470.0 |
| Conductivity, W/(m·K) | 0.33 | 376.7 | 58.1 | 15.0 |

opposed-flow velocity in the range of 4–50 cm/s. The maximum oxygen concentration was limited by the allowable temperature of TC, which would be broken at oxygen concentrations higher than 27%.

The flame-spread rate $V_\mathrm{f}$ was determined from the slope of the flame-front displacement vs. time (the flame-front displacement is linear in time). The temperature profile along the wire core was obtained from the measured $V_\mathrm{f}$ and the core temperature vs. time at a fixed location. The position of the flame front relative to the TC position was defined by images recorded by the digital video camera. Because of the difficulty of measuring the gas-phase preheat zone in the experiment, the origin of the experimental temperature profile was defined at the position of the flame front. Thus, in the analysis of the experimental data, the unburned zone was defined ahead of the spreading flame without defining the uncertain length scale of the preheat zone. At least three tests were repeated for each test condition to obtain reliable results. All experimental data presented in the manuscript were newly acquired in this study.

## 4. Results and discussion

### *4.1. Flame-spread rate*

At first, the flame-spread rate $V_f$ were obtained as a function of the oxygen concentration, opposed-flow velocity $V_g$, and thermal conductivity $\lambda_c$ of the wire core. Figure 4 shows $V_f$ as a function of oxygen concentration under constant opposed-flow velocity ($V_g$ = 4 cm/s): $V_f$ increases monotonically with increasing oxygen concentration irrespective of core material (however, as found in a previous study [22], when oxygen concentration exceeds 25%, $V_f$ for the Cu wire starts to decrease upon further increasing oxygen concentration up to 31% due to a decrease in flame length).

Although Fig. 4 does not show how $V_g$ affects $V_f$ (for clarity), a larger $V_g$ always leads to a smaller $V_f$ under the conditions tested. A similar trend was found in previous studies [17][28]. Note also that a highly conductive wire always leads to faster $V_f$ and lower LOC. These trends are also consistent with the results of previous studies [15][16][17][22][21], except for the results obtained in both microgravity and normal gravity conditions with horizontal configuration [1].

*4.2. Typical temperature profiles along wire core*

Figures 5(a) and (b) show the effect of the core material on the temperature profile along the wire core. The temperature in the unburned zone is higher and its profile is extended further in the upstream direction as $\lambda_c$ increases.

Figures 5(c) and (d) show the effect of oxygen concentration on the temperature profile along the Cu wire. A decrease in oxygen concentration also extends the temperature profile into the upstream

direction, and the same trends were obtained even for Fe and NiCr wires (not shown in the figure). These results are explained by the correlation between $V_{\mathrm{f}}$ and $L_{\mathrm{c}}$ in Eq. (7). As can be seen in Fig. 4, a decrease in oxygen concentration decreases $V_{\mathrm{f}}$ and extends $L_{\mathrm{c}}$. Nakamura *et al.* [29] previously measured the temperature profiles on a solid surface and in the gas phase during downward flame spread over a 4.0-mm-thick slab of polymethylmethacrylate and they found that as the condition of spreading flame approached the extinction limits (i.e., $V_{\mathrm{f}}$ decreases) the length of a preheated region on the solid surface extends into the upstream direction more than that in the gas phase. Then, they pointed out that the forward heat conduction in the solid slab plays an important role in the flame-extinction process even with low-conductivity polymeric materials. In the case of electric wires, this effect must be much more pronounced because of the presence of the metal conductor within the polymeric insulation.

Each temperature profile in Fig. 5 reveals a peak value and an inflection point. The locations of the peak temperature and inflection point correspond to the flame tail (downstream end of the burned zone in Fig. 1(a)) and the burnout edge of the molten LDPE (downstream end of the pyrolysis zone in Fig. 1(a)), respectively. The inflection point suggests that the temperature gradient along the wire core decreases in the pyrolysis zone. Because gasification (bubble generation) of the molten LDPE appears near the downstream end of the pyrolysis zone, we can expect that the wire core acts as a heat source for the molten LDPE and then it turns to be a heat sink in the upstream side of the pyrolysis zone. A similar situation was observed in a numerical study by Umemura *et al.* [6] and experimental studies

by Kobayashi *et al.* [28][30].

The maximum core temperature $T_{\mathrm{c,max}}$ and core temperature $T_{\mathrm{u}}$ ahead of the flame front have unique trends as a function of the ambient oxygen concentration. Figure 6 shows $T_{\mathrm{c,max}}$ and $T_{\mathrm{u}}$ as a function of oxygen concentration under constant opposed-flow velocity ($V_{\mathrm{g}}$ = 4 cm/s). As can be seen in the figure, $T_{\mathrm{c,max}}$ of Cu wire increases with an increase in oxygen concentration from 17% to 21% and then turns to decrease from 21% to 25%. However, Fe and NiCr wires show that $T_{\mathrm{c,max}}$ increases monotonically with oxygen concentration. On the contrary, $T_{\mathrm{u}}$ decreases monotonically with an increase in oxygen concentration and the same trend is found for all tested wires; nevertheless, the flame temperature normally increases with oxygen concentration. These observations are explained by the competition between heat flux from the flame around the wire and the characteristic residence time ($t_{\mathrm{res}} \propto 1/V_{\mathrm{f}}$) of a flame spreading over an electric wire. Because $t_{\mathrm{res}}$ varies inversely with $V_{\mathrm{f}}$, the wire sample is heated by the flame for a longer time as $V_{\mathrm{f}}$ decreases, and vice versa. Therefore, an increase in oxygen concentration accompanied by an increase in $V_{\mathrm{f}}$ can result in a lower $T_{\mathrm{c,max}}$ and $T_{\mathrm{u}}$ even with increased flame temperature. Because the increment rate of $V_{\mathrm{f}}$ with Cu wire is relatively large among all tested wires (see Fig. 4), a regime where $T_{\mathrm{c,max}}$ is controlled by $t_{\mathrm{res}}$ rather than the flame temperature should appear.

*4.3. Comparison between the theoretical and experimental results*

To confirm the validity of the theoretical analysis in section 2, a comparison has been made between the theoretical and experimental results. As discussed previously, the temperature profile in the unburned zone is characterized by the effective heat-diffusion length $L_c$ along a wire core. When we observe the temperature profiles in Fig. 5, we can easily find that those in the unburned zone follow the heat-conduction-controlled distribution. If such presumption is correct the measured temperature profile along the wire core in the unburned zone should follow an Eq. (6) which is an analytical solution of Eq. (4). Then, $L_c$ should be the same between experiment and theory. Now the regression analysis is performed to find the $L_c$ from the measured temperature profiles by using the following equation which is nearly identical to an analytical solution of the temperature profile

$$T_c = T_\infty + C_1 \exp\left(-\frac{x}{C_2}\right), \tag{15}$$

where $C_1$ and $C_2$ are the regression coefficients. Once the best fit curve according to Eq. (15) is found, we can define $L_c$ from the measured temperature profiles because $C_2$ corresponds to $L_c$ in Eq. (6). If the characteristic length determined by the measured temperature profile is consistent with theory, we can justify the discussion in section 2. Several representative results of the regression analysis are shown in Fig. A1 of Appendix. As can be seen in Fig. A1, Eq. (15) well fitted the measured temperature profile in the unburned zone and these results also justify the assumption of a one-dimensional model since the temperature decay in the unburned zone follows the exponential function.

Figure 7 shows experimentally determined $L_c$ and that predicted by Eq. (7) for Cu, Fe, and NiCr wires, both as a function of $V_f$. Note that only the forced convection was considered for theoretical predictions. As can be seen in the figure, the experimentally determined $L_c$ are well consistent with the theoretical results for all tested wires. These results confirm that the theory given in section 2 describes well the heat-transfer process in the unburned zone. According to the experiment and theory, $V_g$ has less effect on $L_c$ than does $V_f$, which suggests that the ambient conditions such as $V_g$ and oxygen concentration influence $L_c$ through the change in $V_f$.

*4.4. Effect of core material on extinction limits*

Providing the theory given in section 2 correctly describes the actual heat transfer process in the unburned zone, $\eta_f$ ( $\equiv V_f/V_{f,crit}$ ) should be an important parameter to discuss the extinction characteristics of the flame spreading over electric wires in the quenching-extinction regime. Therefore, the extinction natures of spreading flame over tested wires are characterized by comparing $\eta_f$ using the measured $V_f$ presented in Fig. 4. Note again that smaller $\eta_f$ results in greater heat loss in the unburned zone as demonstrated by Fig. 2.

Figure 8 shows $\eta_f$ as a function of oxygen concentration for Cu, Fe, and NiCr wires. As can be seen in the figure, only the results of NiCr wire showed larger value, while those of Fe and Cu wires showed smaller value. This tendency implies that the $V_f$ as a function of physical properties of the core material varies almost proportionally with $V_{f,crit}$ for Cu and Fe wires, but not for NiCr wire. This

result can be explained by the presence of two types of flame-spread mode proposed by Nakamura *et al.* [16]: a wire-driven and flame-driven mode. As demonstrated by present and previous studies [15][16][17][22][21], a less conductive wire generally leads to smaller $V_{\mathrm{f}}$ due to a decrease in forward heat conduction through a wire core. However, if the $V_{\mathrm{f}}$ driven by the heat conduction through a wire core is decreased due to a decrease in $\lambda_{\mathrm{c}}$, the transition from the wire-driven mode to the flame-driven mode should eventually take place. Then, $V_{\mathrm{f}}$ is maintained regardless of a decrease in $\lambda_{\mathrm{c}}$, while $V_{\mathrm{f,crit}}$ in Eq. (9) decreases as $\lambda_{\mathrm{c}}$ decreases. Consequently, $\eta_{\mathrm{f}}$ with the flame-driven mode should become larger than that with the wire-driven mode.

As shown in Fig. 8, Cu wire always has smaller $\eta_{\mathrm{f}}$ than NiCr wire at the same oxygen concentration. This result implies that Cu wire can act as a more effective cooling medium than NiCr wire even though the $V_{\mathrm{f}}$ of Cu wire is much greater than that of NiCr wire (see Fig. 4). Therefore, if the extinction is controlled by the heat balance (quenching extinction), Cu wire can better suppress the flammability of insulation material than NiCr wire due to greater heat loss in the unburned zone. In other words, Fig. 8 explains the experimental fact given by Takahashi *et al.* [1] who found that the LOC of Cu wire is larger than that of NiCr wire in microgravity conditions with low external airflow. Further, the difference between LOC for Cu and NiCr wires obtained by horizontal spread in normal gravity [1] is also reasonably understood by combining the present study and previous study which investigated the effect of sample orientation on $V_{\mathrm{f}}$ [21]. According to the experimental results obtained by Hu *et al.* [21], in horizontal spread, buoyancy induced flow inhibits the downstream

spreading flame from enveloping the wire core in the burned zone hence the heat recirculation through a wire core is suppressed. As a result, the difference between $V_{\mathrm{f}}$ for Cu and NiCr wire becomes small in horizontal spread. Therefore, the gap between $\eta_{\mathrm{f}}$ for Cu and NiCr wire in horizontal spread becomes much larger than the results presented in Fig. 8, hence the heat loss from the unburned zone is pronounced in horizontal spread over Cu wire.

As discussed above, the effect of the core material on the quenching extinction can be evaluated by the newly introduced parameter, $\eta_{\mathrm{f}}$. The theoretical analysis revealed that the $V_{\mathrm{f}}$ itself is a crucial value to understand the quenching extinction in electric wires because the ratio of $V_{\mathrm{f}}$ to $V_{\mathrm{f,crit}}$ determines heat loss in the unburned zone. Namely, extinction limits of the flame spreading over electric wires depend on whether $V_{\mathrm{f}}$ is large enough relative to $V_{\mathrm{f,crit}}$ or not. Now a question naturally arises is why the LOC of Cu wire shows smaller value than that of NiCr wire in downward configuration under normal gravity (See Fig. 4 and ref. [22]). This question should be discussed further in future work, but a common understanding is that the finite-rate chemical kinetics controls the flame-extinction mechanism once external flow velocity becomes large, such as in buoyancy-induced flow. As discussed previously, a highly conductive wire leads to greater $V_{\mathrm{f}}$ than a poorly conductive wire, particularly in downward configuration [21]. Therefore, in flame spread over a highly conductive wire, it is supposed that more gaseous fuel is supplied to the reaction zone and forms a more stable and robust flame front due to the increased fuel concentration in the reaction zone. As a result, the flame spreading over a highly conductive wire becomes difficult to blow out. This could be a possible

explanation for lower LOC of Cu wire in the blow-off extinction regime while further discussion should be needed in the future work.

## 5. Conclusions

This study investigates the effect of the core material on the flame spread and its extinction phenomena in electric wires under the assumption of infinite chemical kinetics. Especially, we discussed the previous experimental findings [1] that the LOC of Cu wire is higher than that of NiCr wire despite Cu wire shows faster $V_{\mathrm{f}}$ than NiCr wire.

At first, a theoretical model that describes the temperature profile along an electric wire in the unburned zone is developed and the validity of the model is confirmed by actual temperature measurement along a wire core during downward flame spread. Then, a key-parameter as dimensionless flame spread rate, $\eta_{\mathrm{f}} \equiv V_{\mathrm{f}}/V_{\mathrm{f,crit}}$, is proposed, where $V_{\mathrm{f}}$ is flame spread rate and $V_{\mathrm{f,crit}}$ is given by Eq.(9). By using the parameter, the heat loss mechanism in the unburned zone is evaluated and the theoretical analysis suggests that a decrease in $V_{\mathrm{f}}$ resulting in a decrease in $\eta_{\mathrm{f}}$ is a dominant mechanism of extinction of a flame spreading over an electric wire.

The effect of the core materials on the extinction limits is also discussed by using the key-parameter above. Under the same $V_{\mathrm{f}}$, heat loss in the unburned zone increases as $\lambda_{\mathrm{c}}$ increases because $V_{\mathrm{f,crit}}$ increases with $\lambda_{\mathrm{c}}$ and resulting in smaller $\eta_{\mathrm{f}}$. When the core material is different $V_{\mathrm{f}}$ could be also

different under the same ambient concentration, but by comparing the value of $\eta_{\mathrm{f}}$, we can understand why Cu wire shows higher LOC than NiCr wire in both microgravity and normal gravity with horizontal configuration.

## Acknowledgments

This research was supported by JAXA as a candidate experiment for the third stage use of JEM/ISS titled "Evaluation of gravity impact on combustion phenomenon of solid material toward higher fire safety" (called "FLARE"). This research was also supported by JSPS KAKENHI Grant Number JP19J10187 (Grant-in-Aid for JSPS Research Fellow).

## Appendix A

Some representative results of the regression analysis to obtain the effective heat diffusion length $L_{\mathrm{c}}$ along a wire core from the experimental temperature profile are presented in Fig. A1. Plots and solid lines in the figure indicate experimental data and fitting curves, respectively. The coefficient of determination ($R^2$) for each fitting curve is listed in the legend of Fig. A1.

## References

[1] S. Takahashi, H. Ito, Y. Nakamura, O. Fujita, Extinction limits of spreading flames over wires in microgravity, Combust. Flame. 160 (9) (2013) 1900–1902.

[2] O. Fujita, Solid combustion research in microgravity as a basis of fire safety in space, Proc. Combust. Inst. 35 (3) (2015) 2487–2502.

[3] M. Kikuchi, O. Fujita, K. Ito, A. Sato, T. Sakuraya, Experimental study on flame spread over wire insulation in microgravity, Symp. Combust. 27 (2) (1998) 2507–2514.

[4] O. Fujita, M. Kikuchi, K. Ito, K. Nishizawa, Effective mechanisms to determine flame spread rate over ethylene-tetrafluoroethylene wire insulation: Discussion on dilution gas effect based on temperature measurements, Proc. Combust. Inst. 28 (2) (2000) 2905–2911.

[5] O. Fujita, K. Nishizawa, K. Ito, Effect of low external flow on flame spread over polyethylene-insulated wire in microgravity, Proc. Combust. Inst. 29 (2) (2002) 2545–2552.

[6] A. Umemura, M. Uchida, T. Hirata, J. Sato, Physical model analysis of flame spreading along an electrical wire in microgravity, Proc. Combust. Inst. 29 (2) (2002) 2535–2543.

[7] S. Takahashi, H. Takeuchi, H. Ito, Y. Nakamura, O. Fujita, Study on unsteady molten insulation volume change during flame spreading over wire insulation in microgravity, Proc. Combust. Inst. 34 (2) (2013) 2657–2664.

[8] M. Nagachi, F. Mitsui, J.-M. Citerne, H. Dutilleul, A. Guibaud, G. Jomaas, G. Legros, N. Hashimoto, O. Fujita, Can a spreading flame over electric wire insulation in concurrent flow achieve steady propagation in microgravity?, Proc. Combust. Inst. 37 (3) (2019) 4155–4162.

[9] Y. Konno, Y. Kobayashi, C. Fernandez-Pello, N. Hashimoto, S. Nakaya, M. Tsue, O. Fujita, Opposed-Flow Flame Spread and Extinction in Electric Wires: The Effects of Gravity, External Radiant Heat Flux, and Wire Characteristics on Wire Flammability, Fire Technol. 56 (1) (2020) 131–148.

[10] A.F. Osorio, K. Mizutani, C. Fernandez-Pello, O. Fujita, Microgravity flammability limits of ETFE insulated wires exposed to external radiation, Proc. Combust. Inst. 35 (3) (2015) 2683–2689.

[11] K. Mizutani, K. Miyamoto, N. Hashimoto, Y. Konno, O. Fujita, Limiting Oxygen Concentration Trend of ETFE-Insulated Wires under Microgravity, Int. J. Microgravity Sci. Appl. 35 (1) (2018) 350104.

[12] M. Nagachi, F. Mitsui, J. Citerne, H. Dutilleul, A. Guibaud, G. Jomaas, G. Legros, N. Hashimoto, O. Fujita, Effect of Ignition Condition on the Extinction Limit for Opposed Flame Spread Over Electrical Wires in Microgravity, Fire Technol. 56 (1) (2020) 149–168.

[13] NASA-STD-6001B, Flammability, offgassing, and compatibility requirements and test procedures, 2011.

[14] X. Huang, Y. Nakamura, A Review of Fundamental Combustion Phenomena in Wire Fires, Fire Technol. 56 (1) (2020) 315–360.

[15] N.N. Bakhman, L.I. Aldabaev, B.N. Kondrikov, V.A. Filippov, Burning of polymeric coatings on copper wires and glass threads: I. Flame propagation velocity, Combust. Flame. 41 (1981) 17–34.

[16] Y. Nakamura, N. Yoshimura, H. Ito, K. Azumaya, O. Fujita, Flame spread over electric wire in sub-atmospheric pressure, Proc. Combust. Inst. 32 (2) (2009) 2559–2566.

[17] Y. Nakamura, N. Yoshimura, T. Matsumura, H. Ito, O. Fujita, Opposed-wind Effect on Flame

Spread of Electric Wire in Sub-atmospheric Pressure, J. Therm. Sci. Technol. 3 (3) (2008) 430–441.

[18] S.L. Olson, Mechanisms of Microgravity Flame Spread Over a Thin Solid Fuel: Oxygen and Opposed Flow Effects, Combust. Sci. Technol. 76 (4–6) (1991) 233–249.

[19] S. Takahashi, T. Ebisawa, S. Bhattacharjee, T. Ihara, Simplified model for predicting difference between flammability limits of a thin material in normal gravity and microgravity environments, Proc. Combust. Inst. 35 (3) (2015) 2535–2543.

[20] S. Takahashi, Prediction of Flammability Limit of Flat Materials in Microgravity Environments, Int. J. Microgravity Sci. Appl. 32 (4) (2015) 320403.

[21] L. Hu, Y. Zhang, K. Yoshioka, H. Izumo, O. Fujita, Flame spread over electric wire with high thermal conductivity metal core at different inclinations, Proc. Combust. Inst. 35 (3) (2015) 2607–2614.

[22] Y. Konno, N. Hashimoto, O. Fujita, Downward flame spreading over electric wire under various oxygen concentrations, Proc. Combust. Inst. 37 (3) (2019) 3817–3824.

[23] J.S. T'ien, Diffusion flame extinction at small stretch rates: The mechanism of radiative loss, Combust. Flame. 65 (1) (1986) 31–34.

[24] S. Bhattacharjee, R.A. Altenkirch, The effect of surface radiation on flame spread in a quiescent, microgravity environment, Combust. Flame. 84 (1–2) (1991) 160–169.

[25] T.-K. Oh, J.S. Lee, S.H. Chung, Effect of gas-phase and surface radiation on the structure and extinction of diffusion flames stabilized on a condensed fuel, Int. J. Heat Mass Transf. 37 (18) (1994) 2893–2900.

[26] S. Rybanin, The dependence of the flame spread rate over solid fuel on Damköhler number and heat loss, Symp. Combust. 26 (1) (1996) 1487–1493.

[27] Y. Sano, S. Nishikawa, The heat transfer coefficient of fine wires in air flow, Chem. Eng. 28 (4) (1964) 275–284.

[28] Y. Kobayashi, Y. Konno, X. Huang, S. Nakaya, M. Tsue, N. Hashimoto, O. Fujita, C. Fernandez-Pello, Effect of insulation melting and dripping on opposed flame spread over laboratory simulated electrical wires, Fire Saf. J. 95 (2018) 1–10.

[29] Y. Nakamura, K. Kizawa, S. Mizuguchi, A. Hosogai, K. Wakatsuki, Experimental Study on Near-Limiting Burning Behavior of Thermoplastic Materials with Various Thicknesses Under Candle-Like Burning Configuration, Fire Technol. 52 (4) (2016) 1107–1131.

[30] Y. Kobayashi, X. Huang, S. Nakaya, M. Tsue, C. Fernandez-Pello, Flame spread over horizontal and vertical wires: The role of dripping and core, Fire Saf. J. 91 (2017) 112–122.

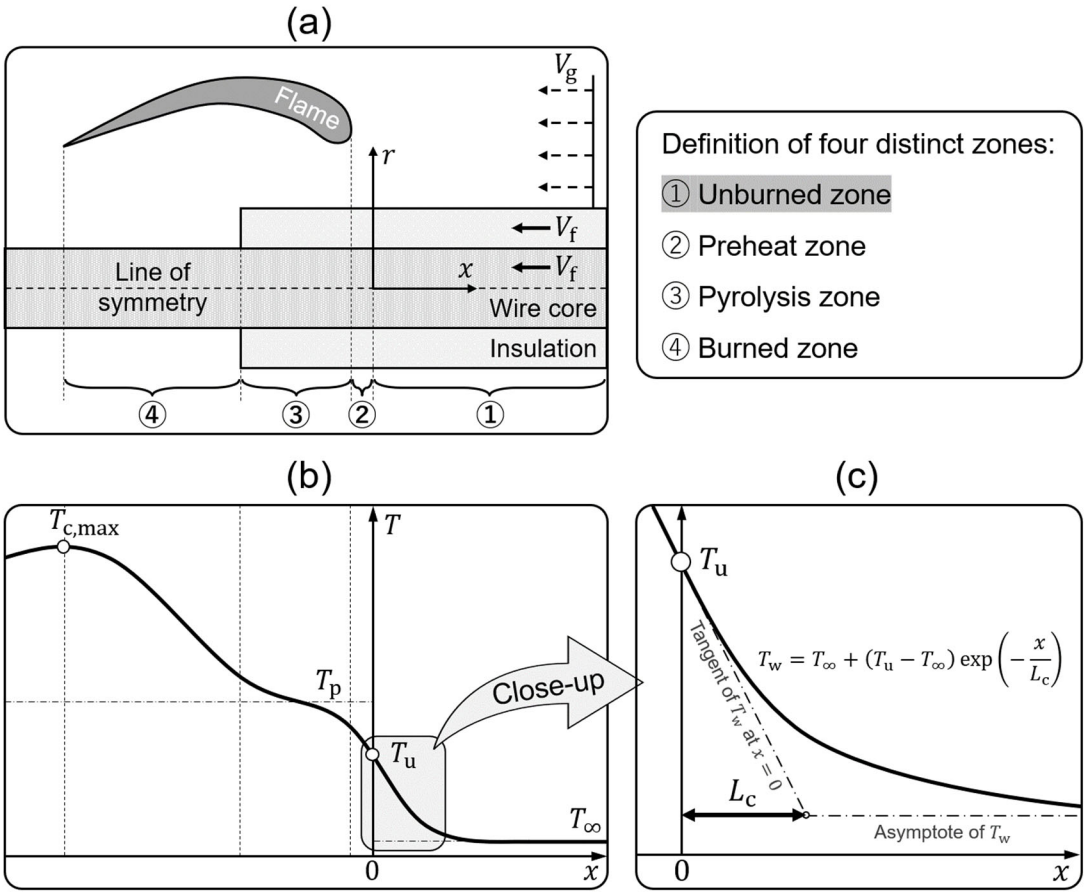


**Fig. 1.** (a) Conceptual description of opposed-flame spread over an electrical wire. (b) Temperature profile along a wire core. (c) The temperature profile in the unburned zone.

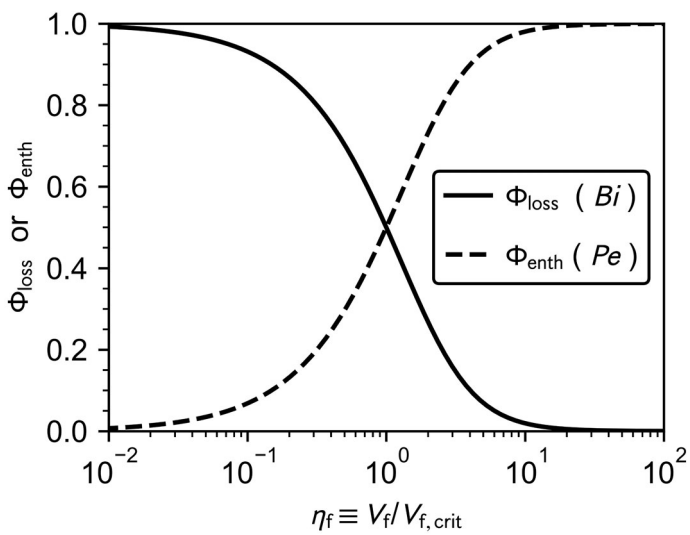


**Fig. 2.** Variations of $\phi_{loss}$ and $\phi_{enth}$ with $\eta_f$.

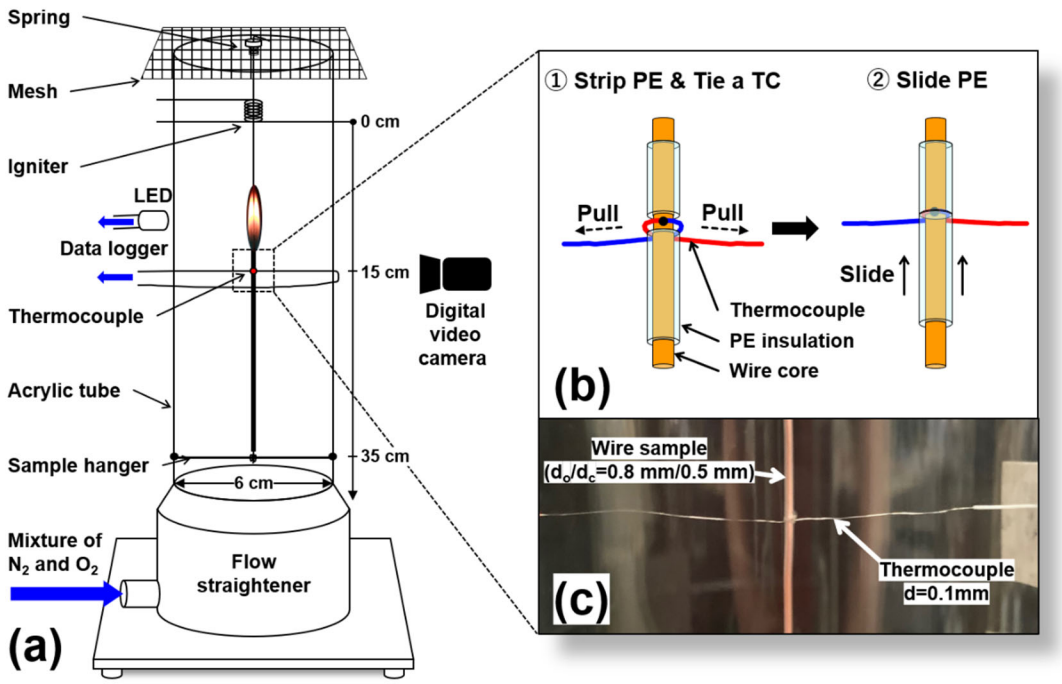


**Fig. 3.** (a) Schematic diagram of experimental apparatus. (b) Illustration of a TC attachment method on the surface of a wire core. (c) Photograph of TC mounted on wire sample.

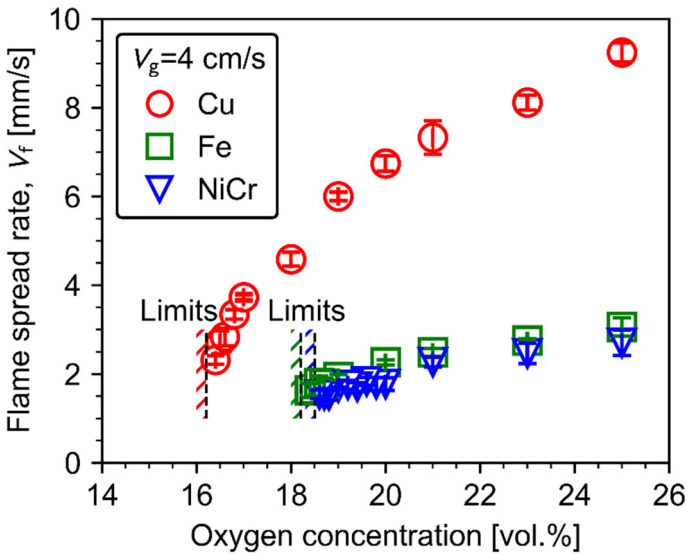


**Fig. 4.** Variations of $V_f$ with oxygen concentration ($V_g$=4 cm/s). Error bars denote the standard deviation of variations between tests.

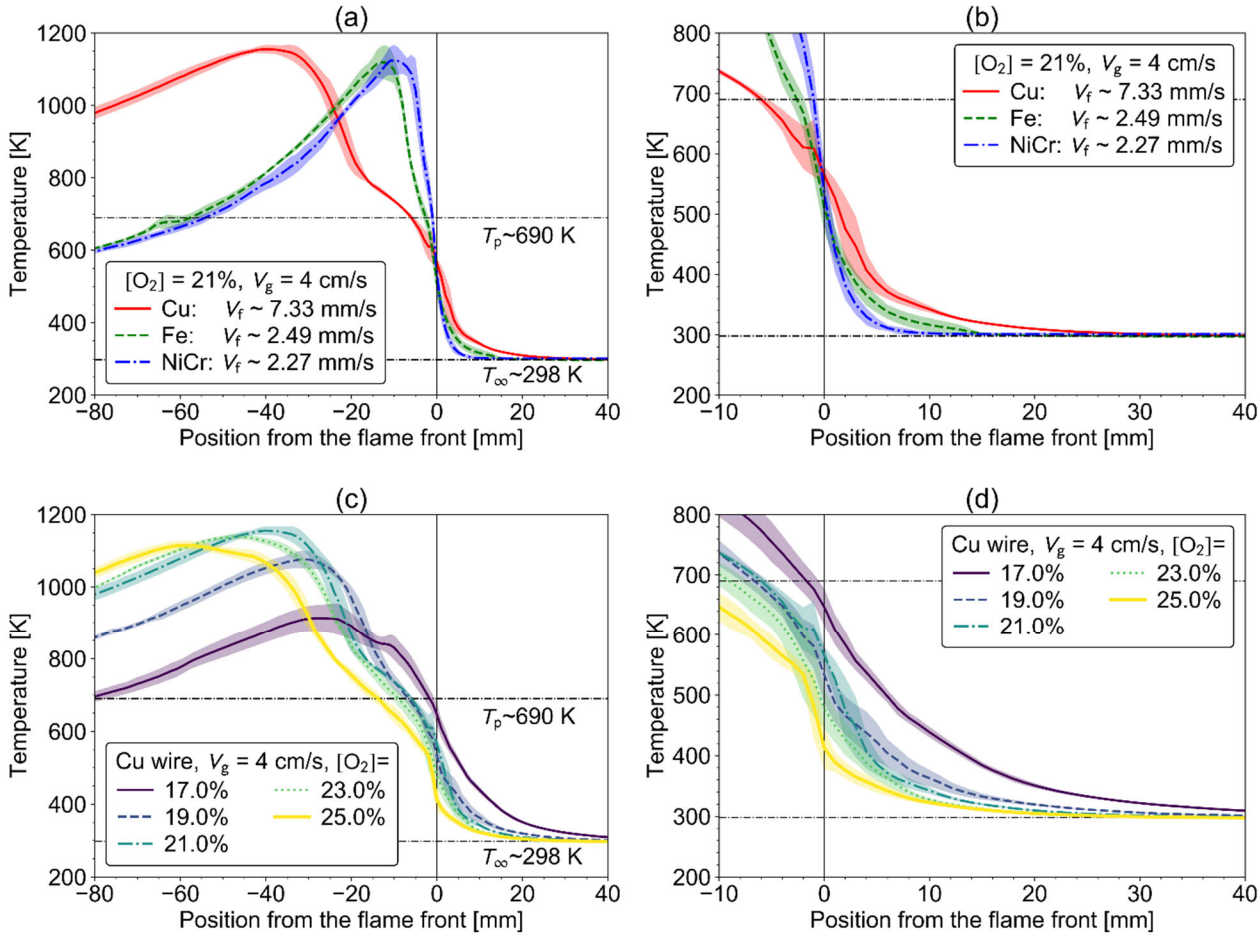


**Fig. 5.** Typical temperature profiles along a wire core. (a) effect of core material at 21% oxygen concentration and 4 cm/s airflow velocity; (b) expanded detail of (a) in the unburned zone; (c) effect of oxygen concentration with Cu wire; (d) expanded detail of (c) in the unburned zone. Each solid line represents averaged data of three repeated tests. Shaded regions indicate the standard deviation of variations between tests. Horizontal dash-dot lines denote pyrolysis temperature $T_p$ of LDPE and ambient temperature $T_\infty$.

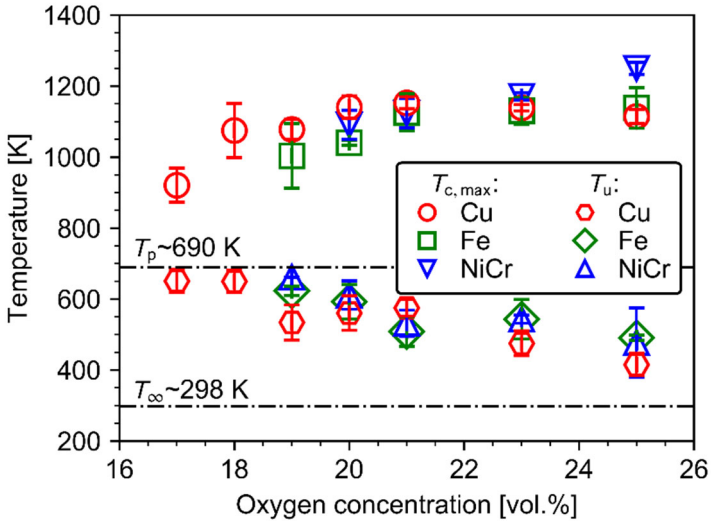


**Fig. 6.** Variations of $T_{c,max}$ and $T_u$ with oxygen concentration ($V_g$=4 cm/s). Error bars denote the standard deviation of variations between tests. Horizontal dash-dot lines indicate pyrolysis temperature $T_p$ of LDPE and ambient temperature $T_\infty$.

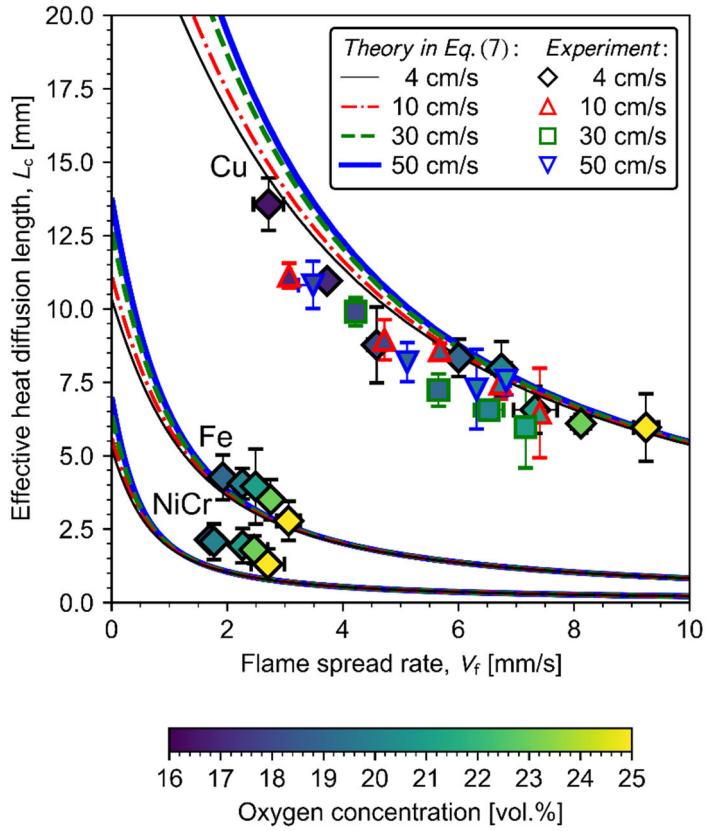


**Fig. 7.** The predictions of $L_c$ from Eq. (7) are compared with the experimental results for Cu, Fe, and NiCr wires. Face and edge colors of each marker represents oxygen concentration and airflow velocity, respectively. Error bars denote the standard deviation of variations between tests.

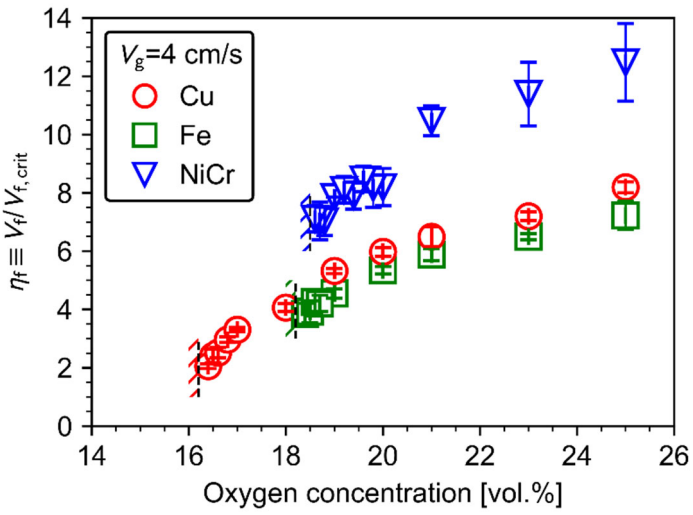


**Fig. 8.** Variations of $\eta_f$ with oxygen concentration ($V_g$=4 cm/s). Error bars denote the standard deviation of variations between tests.

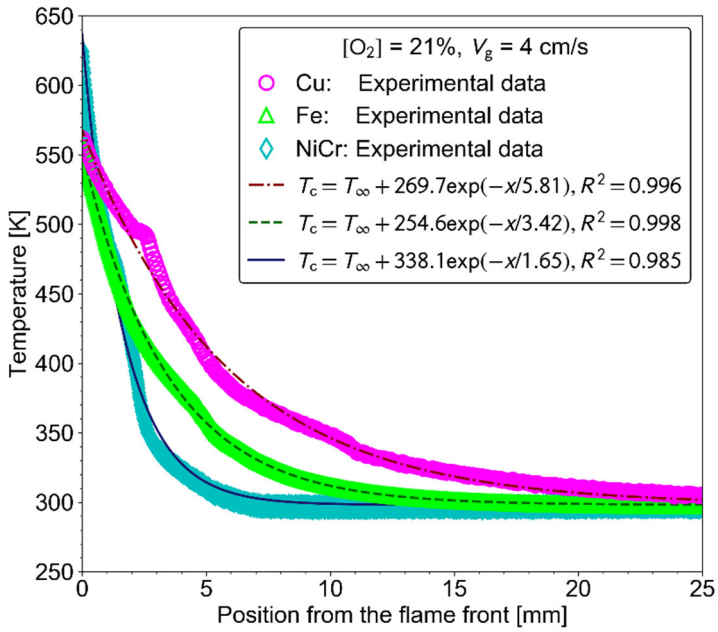


**Fig. A1.** Comparison between the fitting curves and the measured temperature profiles for Cu, Fe, and NiCr wires at 21% oxygen concentration and 4 cm/s airflow velocity.